Mining, Metallurgy & Exploration (2021) 38:2467–2484
https://doi.org/10.1007/s42461-021-00490-z

REVIEW

A Panoramic Overview of Chlorination and Carbochlorination of Light Rare Earth Oxides, Including Thermodynamic, Reaction Mechanism, and Kinetic Aspects

Federico J. Pomiro[1] · Juan P. Gaviría[1,2] · Gastón G. Fouga[1,2] · Ana E. Bohé[1,2,3] · Georgina De Micco[1,2]

Received: 1 June 2021 / Accepted: 9 September 2021 / Published online: 15 October 2021

Abstract
Chlorination and carbochlorination processes have industrial applications in metallurgical activity for extraction and purification of uncommon metals such as rare earth elements (REE). This study reviews the chlorination and carbochlorination reactions of light REE (LREE) oxides with chlorine considering the thermodynamic, stoichiometric, and kinetic aspects of the reactions. Lanthanides between lanthanum to gadolinium were considered as LREE, in agreement with previous literature, and the results were detailed in this review. LREE were analyzed taking into account their oxidation states and were divided into three groups accordingly. The results presented show that, although the LREE are chemically similar, their behaviors during the reactions with Cl_2 and Cl_2–C, and the different LREE-O–Cl compounds formed, have particularities. It was observed that gadolinium, in both thermodynamic calculations and experimental results, presents some differences, and it can be considered intermediate between light and heavy REE; i.e., reactions between $LREE_2O_3$ and $Cl_2(g)$ begin at approximately 250 °C, except for Gd_2O_3 that begins at 327 °C. The present work will contribute to a better understanding of the chemistry of LREE oxides and Cl_2 under different conditions and the products obtained in the LREE–O—$Cl_2(g)$ and LREE–O–C–$Cl_2(g)$ systems.

Keywords Light rare earth oxides · Chlorination · Chlorine · Carbochlorination · Lanthanides · Oxychlorides

1 Introduction

The International Union of Pure and Applied Chemistry (IUPAC) defines as rare earth elements (REE) the set of 17 elements in the periodic table, including the 15 lanthanides between lanthanum and lutetium plus scandium and yttrium [1]. REE are usually divided into low atomic weight elements, lanthanum to europium or gadolinium, referred to as the light rare earth elements (LREE), and heavy rare earth elements (HREE) gadolinium or terbium to lutetium and yttrium. This division is sometimes arbitrary and the term middle REE (MREE) is also used to refer to those elements between europium and dysprosium. The definition of both groups is based on the electron configuration of each REE but sometimes the division may vary according to the considered property by different authors [2]. For example, a difference between these groups is LREE tend to occupy the larger sites of 8–10 coordination number (CN) and occur as carbonates and phosphates, whereas HREE occupy CN: 6–8 sites and are abundant in oxides and a part of phosphates. Based on Shannon's ionic radii, the effective ionic radii of La^{3+}–Gd^{3+}(LREE) for the CN: 8 (anion: oxygen atoms) are 1.18–1.07 Å and those of Y^{3+} and Gd^{3+}–Lu^{3+}(HREE) are 1.015 and 1.07–0.97 Å, in this case gadolinium could be included in both groups [3].

Rare earth elements have attracted particular attention due to their extensive use in many fields [4] and especially in emerging clean technologies and high technology devices. Magnets, the principal application of REE, are used in electronic, automotive, power generation, medical, among other industries. These elements are mostly supplied by China who dominates the REE market because it has the capability to separate and process

✉ Federico J. Pomiro
pomiro@cab.cnea.gov.ar

[1] Departamento de Fisicoquímica y Control de Calidad. Complejo Tecnológico Pilcaniyeu, Centro Atómico Bariloche. Comisión Nacional de Energía Atómica, Av. Bustillo 9500, S.C. de Bariloche, Río Negro, Argentina

[2] Consejo Nacional de Investigaciones Científicas y Técnicas (CONICET), Buenos Aires, Argentina

[3] Centro Regional Universitario Bariloche, Universidad Nacional del Comahue, S.C. de Bariloche, Río Negro, Argentina

the REE concentrate and to manufacture REE-based high performance magnets and electronics [5].

The extreme chemical stability of the rare earth oxides is responsible for the rather complex and energy intensive methods used for rare earth metal production. According to the composition of the rare earth concentrate, different extraction—separation processes have been used involving hydrometallurgy, electrometallurgy, and pyrometallurgy. The exploitation of REE resources is also full of environmental issues. One of the problems is due to radioactive elements such as U and Th associated with REE minerals [6]. This scenario makes it important to develop new strategies for REE production, and chlorination and carbochlorination reactions arise as possible processes to develop methodologies for extraction and purification of these elements from different sources [7].

Since the 1990s, most of Ti and Zr have been obtained by pyrometallurgical processes involving chlorination and carbochlorination reactions [8]. In the past few decades, considerable amounts of Nb and Ta have also been produced by chlorination starting from ferroalloys [9, 10]. Less spread out is the use of chlorination reactions on an industrial scale for waste treatment and recovery of valuable metals from scraps, wastes, and low grade ores, mostly due to economic inefficiency. However, in the literature, there are many studies about chlorination and carbochlorination of ores and metal oxides using different gaseous chlorinating agents (dry method) in a laboratory scale. Among them, there are some related to separation, recovery, and purification of REE. Rare earth chlorides are less volatile than transition metal chlorides, and they have a very similar volatility. For that reason, their separation has been achieved by chemical vapor transport transforming them into volatile complex adducts [11–16]. Some of the chlorination agents used in the studies were Cl_2 [11, 13, 14, 17–37], CCl_4 [38–41], NH_4Cl [42–53], and $ZnCl_2$ [54].

Finally, on a production scale, the Goldschmidt process has been used in Germany since 1967 to obtain REE chlorides. Pellets of bastnaesite ore and carbon were prepared and subsequently chlorinated with Cl_2 at 1000–1200 °C. The chlorides, separated according to their volatility, were free of thorium chloride and any oxychloride and were suitable for the production of the corresponding metal. The process was also convenient for monazite, cerite, xenotime, euxenite, fergusonite, and gadolinite ores.

In view of the state of the art of REE oxide chlorinations, it appears useful and timely to perform an overview of the reactions where Cl_2(g) is used as the chlorinating agent. Xing et al. [55], in their review about application of chlorination processes for ore treatments, only included one work concerning REE ore chlorination with gaseous chlorine. To the best of our knowledge, this paper firstly and comprehensively summarizes a thermodynamics study to determine the thermodynamic viability of the reactions between LREE oxides and chlorine. The published studies about chlorination and carbochlorination of LREE oxides using Cl_2(g) as the chlorinating agent, involve several properties, such as the initial temperature of reaction, identification of the reaction stages, characterization of the products (X-ray diffraction, scanning electronic microscopy, energy dispersive spectroscopy, X-ray fluorescence spectroscopy, Fourier transform infrared spectroscopy, magnetic susceptibility), kinetic determinations, among others.

The reaction that occurs in most of the LREE oxide-chlorine systems is the chlorination of REE_2O_3 to produce REE oxychloride, and the kinetic parameters of this reaction for La, Sm, Nd, Eu, Gd, and Y have already been obtained. In the present review, which is focused in the chlorination and carbochlorination reactions of LREE oxides with Cl_2(g), including lanthanide oxides between lanthanum and gadolinium, previous results are thoroughly analyzed together and compared.

2 General Consideration

For the thermodynamic analysis of the reactions between LREE oxides and chlorine, it is necessary to subdivide this group according to the possible oxidation states that the lanthanide can acquire. In general, all lanthanides have the 3+ oxidation state as dominant; however, deviations are observed throughout this group. Thus, some LREE are only observed with this oxidation state (3+), and others can be with 4+ and/or 2+ oxidation states. It should be noted that promethium will not be analyzed because this element is not present in nature [56].

Thermodynamic calculations were performed using the HSC Chemistry 6.1 software for Windows [57].

Group 1: In this group LREE with 3+ as the only possible oxidation state are considered, either in inorganic materials (oxides, salts, etc.) or as ionic species in solution (Ln^{3+}). As long as the electronic structure of lanthanum is $[Xe]5d^16s^2$, it is easy to explain the existence of the 3+ oxidation state because it corresponds to the loss of the three outer electrons. Assuming that the $5d^16s^2$ electrons were retained across the series of atoms from $[Xe]5d^16s^2$ to $[Xe]4f^{14}5d^16s^2$ and that moving across the lanthanoids corresponds to filling the 4f shell, the predominance of the 3+ oxidation state could be explained as: each atom could lose the $5d^16s^2$ electrons to form the tripositive ion. In this work, lanthanum and gadolinium are considered LREE of group 1.

Group 2: A deviation from the 3+ rule as the most stable oxidation state is cerium, which exhibits the 4+ state as the most stable in oxide (CeO_2) and in solution (Ce^{4+}). This element achieves the electronic configuration of the noble gas xenon, which has high electronic stability. Also praseodymium can be located in this group, which forms oxides and other compounds with mixed oxidation states between 3+ and 4+,

being Pr_6O_{11} and minerals with a similar 3+/4+ ratio found in nature.

This behavior is shown in Fig. 1, which are the phase stability diagrams of the Ln–O systems at constant partial pressure of nitrogen ($pN_2(g) = 10^{-20}$ atm) as inert gas for Ln : Ce and Pr. By lowering the partial pressure of O_2(g), the oxidation states vary from Ln^{4+} to Ln^{3+}, enabling the production of a family of oxides: LnO_2, Ln_xO_y, Ln_2O_3, where Ln_xO_y represents oxides with mixed oxidation states Ln^{3+} and Ln^{4+}. Considering an oxygen pressure of 1 atm, it can be observed that the predominant stability area for Ce is CeO_2 for all temperature ranges, and for Pr is PrO_2 for temperatures lower than 500 °C, and Pr_6O_{11} between 500 and 1000 °C. The praseodymium-oxygen system is notable for its multiple stoichiometries and several intermediate oxidation products have been reported, usually using a general formula PrO_{2+x}.

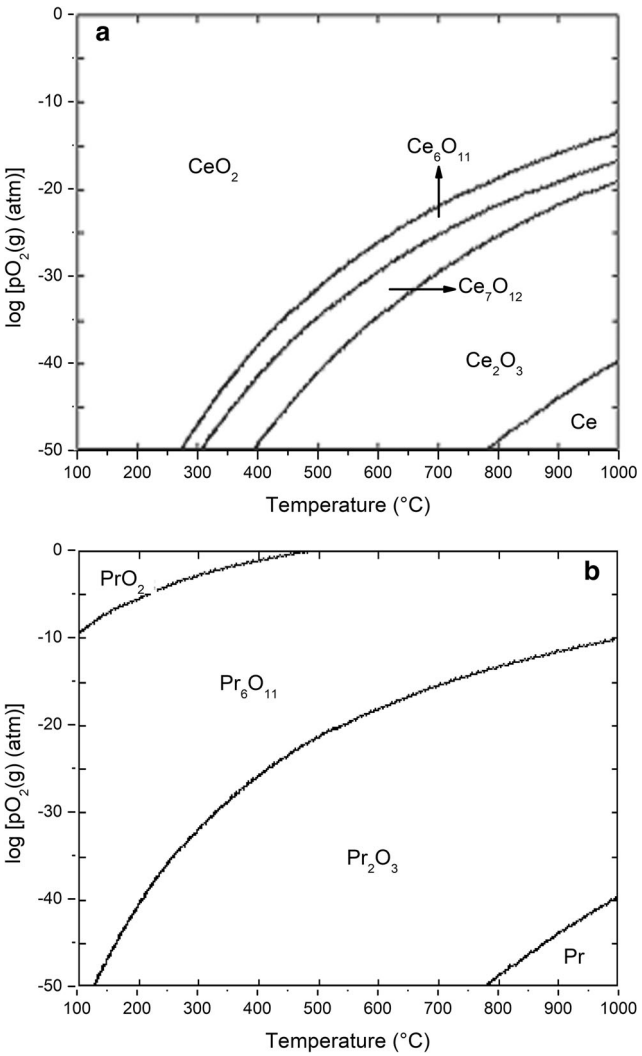

Fig. 1 TPP diagrams of the **a** Ce–O and **b** Pr–O systems for temperatures between 0 and 1000 °C

It is noticed that when the oxygen potential is lowered, mixed oxides are formed in the studied temperature range, and subsequently, Ln_2O_3 is formed. Finally, metal Ln is observed at log $pO_2(g) < -50$ and at approximately 780 °C in both lanthanides.

As shown in the phase stability diagram, the oxidation of lanthanide is a four-step reaction for cerium and a three-step reaction for praseodymium that involves the oxidation reaction of metal to oxides with oxidation state 3+ (Ln_2O_3), subsequently, the oxidation of Ln_2O_3 to form oxides with mixed oxidation state 3+ and 4+. Finally, the formation of oxide with Ln^{4+} is observed (LnO_2) by reaction of O_2(g) with mixed oxides. The mixed oxides are Ce_7O_{12} and Ce_6O_{11}, and Pr_6O_{11} for Ce and Pr systems, respectively.

Group 3: The special characteristic of the LREE of this group is that they can present the 2+ oxidation state in addition to 3+. Neodymium, samarium, and europium can be found in this group. Europium exhibits the 2+ state, achieving the stability of a half-full shell. This characteristic is also observed in the phase stability diagram for europium (Fig. 2), where an area of stability is observed for the oxide with oxidation state 2+ (EuO) for partial pressures of oxygen between 10^{-50} and 10^{-30} atm and temperatures between 525 °C and 1000 °C, respectively. The presence of LnO is not observed for neodymium and samarium in the range of temperatures and pressures analyzed. Europium monoxide is known, but there are doubts about the existence of other low oxygen species. Furthermore, this property of europium can also be seen comparing the ΔG^0_f (formation Gibbs free energy change) for lanthanide sesquioxides. There is a gradual decrease in this value with increasing atomic number Z (from −1508.8 to −1538.8 kJ mol^{-1} for La and Gd, respectively), except for Eu_2O_3, which has a higher ΔG^0_f value (−1355.1 kJ mol^{-1}) than the other LREE.

3 Chlorination Reaction with Chlorine

3.1 Thermodynamics Analysis

3.1.1 Phase Stability Diagrams

The phase stability diagrams show stability (predominance) areas of condensed phases in a ternary system under isothermal conditions, with the remaining constraints as the other axis. These diagrams are very useful when a fast estimation of the prevailing phases is needed. It is assumed that all phases are pure substances. Mixed phases are not taken into account in basic phase stability diagrams. Moreover, phase diagrams are valuable tools for understanding the complex solid-state phase transformations in multicomponent systems, for example, to find the best conditions for chlorination reactions in the present review.

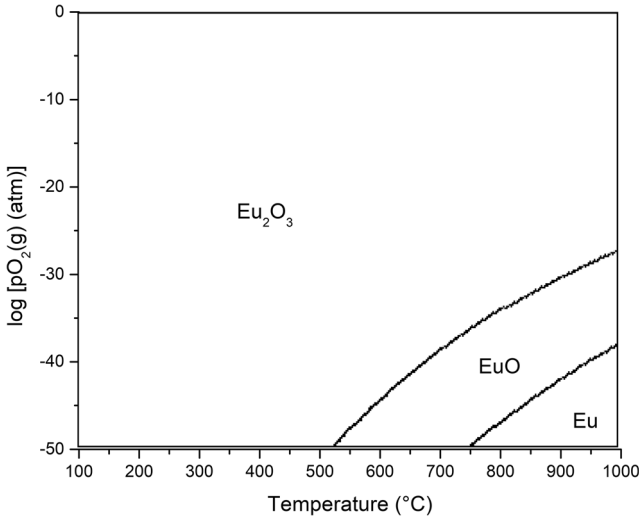

Fig. 2 TPP diagram of the Eu–O for temperatures between 0 and 1000 °C

The phase stability diagrams are calculated taking into account a series of reactions between the condensed phases and their feasibility to occur according to their ΔG at 400 °C and varying partial pressures of chlorine and oxygen. This temperature was chosen because different studies have reported that several chlorination reactions of uncommon metal oxides such as LREE, transition metals such as zirconium and iron oxides, among others, can occur at that temperature [43, 58].

Group 1: La and Gd The reacting system considered has $O_2(g)$–$Cl_2(g)$ atmosphere and solid phases containing Ln for Ln : La, Gd. The following reactions were taken into account for calculating the phase stability diagrams:

$$Ln(s) + 3/2\ Cl_2(g) = LnCl_3(s) \quad (1)$$

$$2Ln(s) + 3/2\ O_2(g) = Ln_2O_3(s) \quad (2)$$

$$Ln(s) + 1/2\ Cl_2(g) + 1/2\ O_2(g) = LnOCl(s) \quad (3)$$

$$Ln_2O_3(s) + 3Cl_2(g) = 2LnCl_3(s) + 3/2\ O_2(g) \quad (4)$$

$$LnOCl(s) + Cl_2(g) = LnCl_3(s) + 1/2\ O_2(g) \quad (5)$$

$$1/2Ln_2O_3(s) + 1/2Cl_2(g) = 1/4\ O_2(g) + LnOCl(s) \quad (6)$$

Figure 3 shows the stability field diagram of ternary Ln–O–Cl computed from thermodynamic data for Ln: La and Gd. It is noticed that the stable condensed phases at 400 °C for these systems are metal and oxide (Ln_2O_3), oxychloride (LnOCl), and chloride ($LnCl_3$) in which the lanthanide has a 3+ oxidation state, in agreement with previous considerations. There are two invariant points (triple points) in the diagram: (a) Ln-Ln_2O_3-LnOCl, which results from the intersection of the equilibrium lines Ln-Ln_2O_3 and Ln_2O_3-LnOCl; and (b) Ln-LnOCl-$LnCl_3$, which results from the intersection of the equilibrium lines Ln-LnOCl and LnOCl-$LnCl_3$.

In a chlorination reaction under experimental conditions such as pCl_2 = 1 atm (log pCl_2 = 0) and 400 °C, according to the stability diagrams, $LnCl_3$ is the most stable species when log $pO_2(g) < 0$, while for higher oxygen partial pressure it is LnOCl. The diagram indicates that Ln_2O_3 and $LnCl_3$ do not have a thermodynamic equilibrium; consequently, LnOCl has to be formed prior to the formation of $LnCl_3$ from Ln_2O_3. Hence, the chlorination reaction of Ln_2O_3 with direct formation of $LnCl_3$ and $O_2(g)$ evolution does not represent a true equilibrium. As can be seen, the region of Ln and $LnCl_3$ (which involves reaction 1) only depends on pCl_2, whereas the equilibriums between Ln_2O_3 and LnOCl (reaction 6) and LnOCl and $LnCl_3$ (reaction 5) depend on both $pO_2(g)$ and $pCl_2(g)$. These two lines have a slope of 2. There are some differences between the La and Gd systems, mainly in the equilibrium between the phases Ln_2O_3 and LnOCl, which is shifted to higher values of pCl_2 in the Gd system. This means that a higher value of chlorine partial pressure is needed to carry out reaction 6 for the lanthanide oxide with higher atomic number, being possible at log pCl_2 around −15 and −6 for La and Gd, respectively, when log pO_2 = 0.

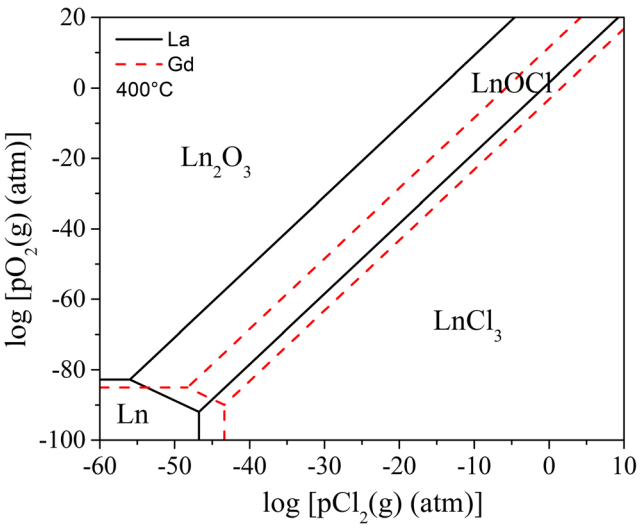

Fig. 3 Phase stability diagram for ternary Ln–O–Cl systems (Ln: La, Gd) at 400 °C

Group 2: Ce and Pr Figure 4 shows the stability field diagram for the ternary Ln–O–Cl system, computed with the thermodynamic data from Ln: Ce and Pr. The condensed phases stable at 400 °C are the same as for group 1, and the oxides are LnO_2 and Ln_7O_{11} (for praseodymium Pr_6O_{11} was considered in the calculations but is not thermodynamically feasible to be formed).

In addition to the reactions discussed for group 1, the following reactions should be taken into account for Ln : Ce, Pr due to the presence of compounds with 4+ oxidation state such as mixed oxides and LnO_2:

$$Ln(s) + O_2(g) = LnO_2(s) \quad (7)$$

$$7Ln(s) + 6O_2(g) = Ln_7O_{12}(s) \quad (8)$$

$$LnO_2(s) + 3/2\ Cl_2(g) = LnCl_3(s) + O_2(g) \quad (9)$$

$$7LnCl_3(s) + 6O_2(g) = Ln_7O_{12}(s) + 21/2\ Cl_2(g) \quad (10)$$

$$LnO_2(s) + 1/2\ Cl_2(g) = LnOCl(s) + 1/2\ O_2(g) \quad (11)$$

$$Ln_7O_{12}(s) + 7/2\ Cl_2(g) = 7\ LnOCl(s) + 5/2\ O_2(g) \quad (12)$$

$$Ln_2O_3(s) + 1/2\ O_2(g) = 2\ LnO_2(s) \quad (13)$$

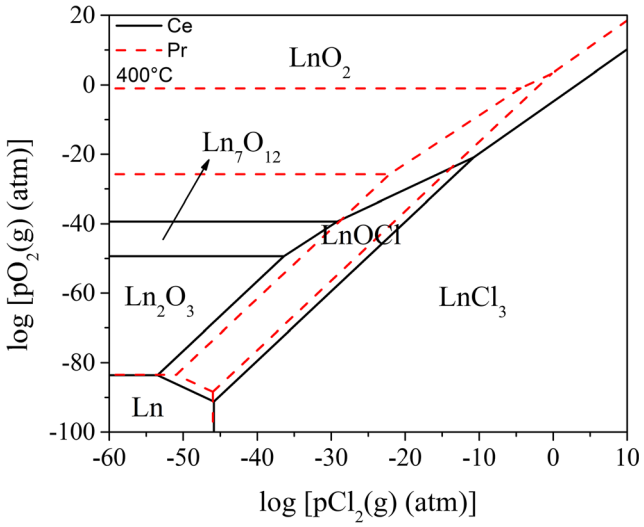

Fig. 4 Phase stability diagram for ternary Ln–O–Cl systems (Ln: Ce, Pr) at 400 °C

$$Ln_7O_{12}(s) + O_2(g) = 7LnO_2(s) \quad (14)$$

$$7/2Ln_2O_3(s) + 3/4\ O_2(g) = Ln_7O_{12}(s) \quad (15)$$

Formation of lanthanide tetrachlorides is not included in the analysis because no conclusive evidence on their existence has been reported and no simple lanthanide tetrachlorides are known [56, 59, 60].

There are five triple points in the diagram: two of them were also observed in group 1 (Ln-$LnCl_3$-LnOCl; Ln-LnOCl-Ln_2O_3) and the other three are due to the presence of compounds of Ln^{4+}: $LnCl_3$-LnOCl-LnO_2; LnOCl-LnO_2-Ln_7O_{12}, and LnOCl-Ln_2O_3-Ln_7O_{12}. As can be seen, the oxide regions (Ln_2O_3, Ln_7O_{12}, and LnO_2) depend only on pO_2 and the equilibrium between these phases is in agreement with the oxides stability diagrams (Fig. 1). The equilibrium regions LnOCl and $LnCl_3$ depend on both $pO_2(g)$ and $pCl_2(g)$.

The diagram indicates that neither Ln_2O_3 nor Ln_7O_{12} have thermodynamic equilibrium with $LnCl_3$. For that reason, LnOCl has to be formed prior to the formation of $LnCl_3$ from Ln_2O_3 and Ln_7O_{12} with evolution of $O_2(g)$ through reactions 6 and 12, respectively. Moreover, if the pO_2 is high enough, formation of oxides in high oxidation states through reactions 13 and 14 is possible, followed by formation of $LnCl_3$ and $O_2(g)$ evolution according to reaction 9. In this group, unlike group 1, thermodynamic equilibrium between the oxides and $LnCl_3$ exists at $\log pO_2 > -20.9$ and 3.2 and $\log pCl_2 > -10.7$ and −0.2 for CeO_2 and PrO_2, respectively.

Group 3: Nd, Sm, and Eu In addition to the reactions presented in group 1, the following reactions should be taken into account for Ln : Nd, Sm, Eu due to the existence of chlorides with 2+ oxidation state ($LnCl_2$), to calculate the Kellogg stability field diagram of Fig. 5:

$$Ln(s) + Cl_2(g) = LnCl_2(s) \quad (16)$$

$$LnCl_2(s) + 1/2\ Cl_2(g) = LnCl_3(s) \quad (17)$$

$$Ln_2O_3(s) + 2Cl_2(g) = 2LnCl_2(s) + 3/2O_2(g) \quad (18)$$

$$LnOCl(s) + 1/2Cl_2(g) = LnCl_2(s) + 1/2O_2(g) \quad (19)$$

For Eu, the oxide EuO should be included, which can involve the following reactions:

$$Eu(s) + 1/2\ O_2(g) = EuO(s) \quad (20)$$

$$EuO(s) + Cl_2(g) = EuCl_2(s) + 1/2\ O_2(g) \quad (21)$$

$$EuO(s) + 3/2\ Cl_2(g) = EuCl_3(s) + 1/2\ O_2(g) \quad (22)$$

$$2\ EuO(s) + 1/2\ O_2(g) = Eu_2O_3(s) \quad (23)$$

$$EuO(s) + 1/2\ Cl_2(g) = EuOCl(s) \quad (24)$$

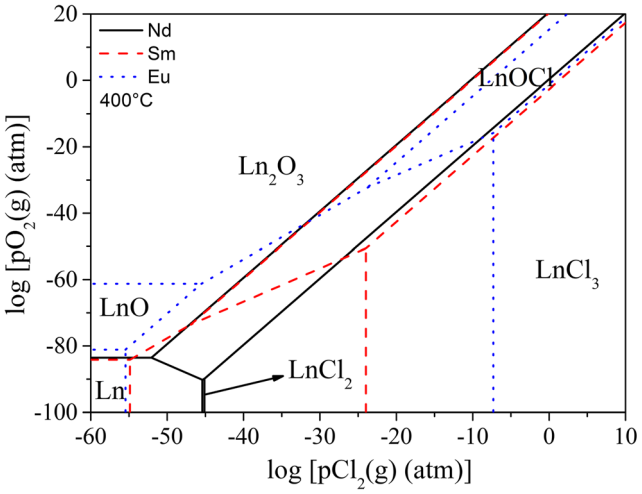

Fig. 5 Phase stability diagram for ternary Ln–O–Cl systems (Ln: Nd, Sm, Eu) at 400 °C

For Nd and Sm, three triple points were determined, one in addition to those in group 1, which is $LnCl_2$-$LnCl_3$-LnOCl. For Eu the triple points calculated are different due to the presence of EuO in the diagram (Eu-$EuCl_2$-EuO; $EuCl_2$-$EuCl_3$-EuOCl; $EuCl_2$-EuO-Eu_2O_3; $EuCl_2$-Eu_2O_3-EuOCl).

3.1.2 ΔG Comparison of Ln_2O_3 and LnOCl Chlorination

Figure 6 shows the Ellingham diagram for reaction 6 that summarizes the evolution of the standard free energy changes per mol of chlorine, ΔG^0, as a function of temperature between 0 and 1000 °C. This reaction has been experimentally identified and reported in several chlorination studies [17–24]. Furthermore, for Ln_2O_3 under chlorine atmosphere, reaction 6 is thermodynamically the most feasible reaction to occur according to previous discussion. For that reason, its analysis is important.

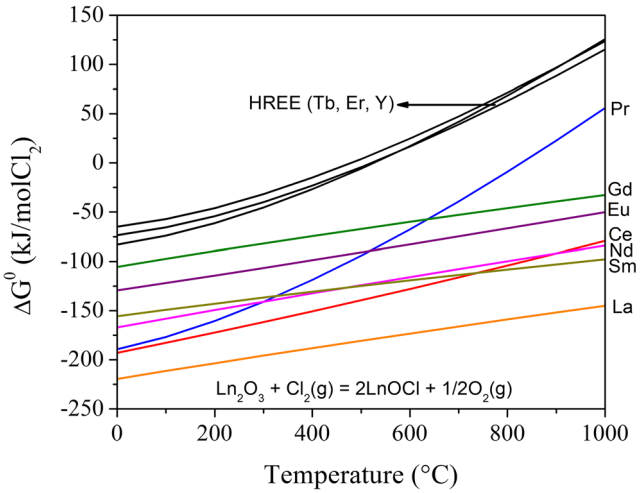

Fig. 6 ΔG^0 vs. T for reactions of Ln_2O_3 with Cl_2(g) with formation of LnOCl between 0 and 1000 °C

When comparing the energy of multiple reactions involving the same set of species within a given system, those with lower Gibbs free energy value would preferentially occur; this concept is used to theoretically predict the behaviors in the systems of the present work. However, experimental results could change due to kinetic aspects.

For a better understanding, HREE oxides (Tb_2O_3, Er_2O_3 and Y_2O_3) were considered in addition to the oxides discussed above (LREE oxides).

The first observation is that all Ln_2O_3 (Ln: LREE) chlorination reactions with LnOCl formation are feasible thermodynamically in all the temperature ranges studied (they have $\Delta G°$ value lower than zero), except for Pr_2O_3 chlorinations, which have $\Delta G° > 0$ at temperatures higher than 825 °C. It can be seen that for these reactions, the $\Delta G°$ value decreases with Z for T < 300 °C, while for T > 300 °C there are some deviations, mainly in oxides of group 2 (Ce and Pr). When the HREE oxides are included in the analysis, in contrast to LREE, these elements have a very similar behavior; the reactions have $\Delta G° < 0$ for temperatures lower than approximately 500 °C and $\Delta G° > 0$ for higher temperatures. Furthermore, $\Delta G°$ values for LREE oxide chlorinations are lower than those for HREE, indicating that chlorination reactions of LREE are thermodynamically more feasible to occur than chlorination of HREE. This difference can also be considered when defining the division between REE and to include gadolinium in the LREE group.

In a flow reactor, the expected products to be formed can be analyzed considering the following equations that relate the standard-state Gibbs free energy of reaction with the Gibbs free energy at any point in a given reaction (not necessarily at standard-state conditions):

$$\Delta G_r = \Delta G^0 + \mathrm{RT}\ln Q \tag{25}$$

Being Q for solid–gas reactions (considering the activities of pure condensed species equal to 1):

$$Q = \frac{\prod_p p_p^i}{\prod_r p_r^j} \tag{26}$$

With $\prod_r p_r^j$ the product of the partial pressures of the gaseous reaction reactants raised to each stoichiometric coefficient j for a given reaction and $\prod_p p_p^i$ the product of the partial pressures of the gaseous products raised to each stoichiometric coefficient i. By understanding the relationship of Q, and equilibrium constant K, one can shift the equilibrium in order to enhance product formation by increasing the number of moles of reactants or by continuously removing the products.

In reaction 5, all gaseous reaction products are removed from the reaction vessel by the flow of reactant gas (which can be considered constant), thus reducing the value of Q. For this reason, reaction 5 was analyzed according to Eq. 25

and 26. During LnOCl chlorination in a continuous flow reactor, the partial pressures of the reaction products will tend to zero if they occur with $LnCl_3$ evaporation, whereas the partial pressure of the chlorination agent will remain constant.

For this reason, ΔG_r values were calculated for temperatures higher than 700 °C, using $LnCl_3$ vapor pressure values, which allow its evaporation during LnOCl chlorination (reaction 5). This partial pressure of gaseous products was chosen taking into account the order of the O_2 partial pressure value in commercial nitrogen or argon gases used as purge gas before chlorination reactions, and is also in the order of the vapor pressure values of the chlorides at the temperatures considered. Table 1 shows ΔG_r values calculated for product pressures of 10^{-4} atm and La, Nd, and Gd systems (as examples of extreme and intermediate LREE). It can be observed that reaction 5 can occur for temperatures higher than 700, 800, and 900 °C for La, Nd, and Gd systems, respectively, due to the equilibrium displacement according to Le' Chatelier principles caused by the removal of gaseous species. These results indicate that chlorination reactions of LREE oxychloride with trichloride formation are thermodynamically more feasible to occur when LREE atomic number decreases; this behavior is important to be considered for separation of LREE chlorides using chlorination with Cl_2(g).

3.2 Analysis of Experimental Results

3.2.1 Preliminary Considerations: Initial Sample and Reaction Equipment

In order to compare the chlorination reactions of different LREE oxides, it is necessary for the reaction conditions to be equivalent. For this reason, effects that influence solid–gas reactions should be known such as initial mass, sample morphology and purity, gas reaction flow rates and partial pressures, role of mass transport processes (whether they influence the global reaction or not), among others.

There are studies about chlorination of LREE oxides, mainly $LREE_2O_3$, also called sesquioxides, and several of them were carried out in our laboratory such as La_2O_3, Nd_2O_3, Pr_2O_3, Sm_2O_3, Eu_2O_3, and Gd_2O_3 [17–23]. In addition, chlorination studies of others oxides have been published such as CeO_2 and praseodymium mixed oxides [23, 25].

Table 1 ΔG_r for LnOCl chlorination with Cl_2(g) and formation of $LnCl_3$

ΔG_r(kJ mol^{-1}) T (°C)	La	Nd	Gd
700	−14.2	21.0	29.9
800	−41.5	−4.5	4.6
900	−68.7	−29.8	−20.5
1000	−95.7	−55.0	−45.4

$LREE_2O_3$ are unstable in air at ambient conditions, forming hydroxides and oxycarbonates, especially La, Nd, and Pr. Decomposition of lanthanide hydroxides begins to occur at approximately 200 °C and proceeds through two reactions (except for Ce and Pr):

$$Ln(OH)_3(s) = LnOOH(s) + H_2O(g) \quad (27)$$

$$LnOOH(s) = 1/2\ Ln_2O_3(s) + 1/2\ H_2O(g) \quad (28)$$

Whereas decomposition of lanthanide oxycarbonate begins to occur at approximately 600 °C and progresses through the following reaction:

$$Ln_2O_2CO_3(s) = Ln_2O_3(s) + CO_2(g) \quad (29)$$

Various investigations have been carried out to study the decomposition of lanthanum hydroxide or oxycarbonate and of neodymium hydroxide or oxycarbonate. Haibel et al. studied the decomposition of carbonated lanthanum hydroxide ($La(OH)CO_3$). Two reactions were identified as thermal decomposition of $La(OH)_3$ and thermal decomposition of $La(OH)CO_3$ [17, 61].

When oxides of group 2 (Pr and Ce) are calcinated at high temperature in air, their behavior is different from the above discussed because stable oxides CeO_2 and Pr_6O_{11} are obtained. Pr_2O_3 was synthesized by reaction of Pr_6O_{11} in Ar-5% H_2(g) atmosphere at 970 °C; Pr_2O_3 and Pr_6O_{11} are the only praseodymium oxides stable at room temperature and these two oxides were used in the chlorination studies [23].

Due to their room temperature instability, the analytical oxides used for chlorination studies between [17, 24] were treated at temperatures higher than 600 °C before the chlorination reactions [17–24]. The initial oxides after calcinations treatments were morphologically characterized by scanning electron microscopy and, in general, the initial sesquioxides were formed by particles with sizes lower than 10 μm.

Various studies have been conducted on the crystalline structure of REE sesquioxides and their phase transformations. Below 2000 °C, the sesquioxides can exist in three crystal systems: the cubic C-type, the monoclinic B-type, and the hexagonal A-type. With increasing temperature, the stability of the structures is generalized by the order C → B → A. Under ambient conditions, the A-type oxide is preferred for lanthanum to promethium, while samarium, europium, and gadolinium can adopt either the B or C-type structures. The crystal structure of the B-type is known to be stable in Sm_2O_3, Eu_2O_3, and Gd_2O_3 above temperatures of 800, 1200, and 1400 °C, respectively, at normal pressure. Usually, chlorinations of LREE oxides were carried out at temperatures lower than phase transition of oxides as will be detailed later [62, 63].

Typical non-isothermal and isothermal thermogravimetric analysis (TGA) under chlorine/argon atmosphere, using a thermobalance, have been performed to study LREE oxides chlorination. Generally, non-isothermal reactions are carried out to determine initial temperature, reactivity, and reaction stages, and isothermal reactions are used to obtain kinetic parameters such as activation energies, reaction order, and reaction models. The chlorination reactions discussed in the present review were studied using the same experimental system (TGA), except for praseodymium oxides chlorinations [23], which were analyzed by gravimetry and XRD-Rietveld analyses using a fixed-bed reactor.

The abovementioned strategy for analyzing thermal analysis data is sophisticated and requires a deep insight into the processes taking place inside the thermal analysis apparatus.

3.2.2 Initial Temperature and Reaction Stages for $LREE_2O_3$–Cl_2(g) Systems

From non-isothermal reaction for $LREE_2O_3$ chlorinations with Cl_2(g), the initial temperatures were determined and the results indicated that these reactions begin at approximately 250 °C for La, Pr, Nd, Sm and Eu, and at 327 °C for Gd. Only one HREE sesquioxide was chlorinated (Y_2O_3 [24]) with Cl_2(g), and this reaction begins at 600 °C. The initial temperature for $LREE_2O_3$ chlorination with Cl_2(g) can also be considered in defining the division between REE; gadolinium being an element intermediate between LREE and HREE. All these reactions start with mass gain until temperatures above 850 °C, where their behavior switches to mass loss.

In agreement with the relative mass changes observed in TG data, for La_2O_3, Nd_2O_3, Sm_2O_3, Eu_2O_3, and Gd_2O_3, the reactions involved are the following:

$$Ln_2O_3(s) + Cl_2(g) = 2LnOCl(s) + 1/2O_2(g) \quad (30)$$

$$LnOCl(s) + Cl_2(g) = LnCl_3(l) + 1/2O_2 \quad (31)$$

$$LnCl_3(l) = LnCl_3(g) \quad (32)$$

The only solid compound obtained is oxychloride for all the investigated $LREE_2O_3$–Cl_2 systems. No trichloride was ever observed in the crucible in any stage of these reactions, indicating that the rate of reaction 31 is lower than the rate of reaction 32. Moreover, chloride evaporation is enhanced due to the gas flow condition during the chlorination reactions.

The proposed mechanism has been confirmed with experiments in which the flow of chlorine was cut off after some time of reaction while maintaining the sample at high temperature in Ar. Under argon atmosphere, no further mass change was observed, and the product in the crucible after cooling was found to be oxychloride (confirmed by XRD). These results demonstrated that the mass loss occurring in chlorine is not due to oxychloride decomposition but is due to oxychloride chlorination and subsequent chloride evaporation. The highest temperature analyzed under argon atmosphere was 950 °C, showing that until that temperature, the oxychlorides of La, Eu, Nd, and Gd are stable.

Oxychloride chlorination given by reaction 31 occurs at temperatures higher than 800 °C (i.e, La [17], Eu [21], Gd [22]). In previous studies from our laboratory, it was determined that in the thermogravimetric experimental setup under a continuous flow that removes the gaseous products, volatilization is significant when the vapor pressure of the chloride exceeds a value of 10^{-4} atm [64]. Figure 7 shows the vapor pressure of $LnCl_3$ calculated from the equilibrium constant of reaction 32. The corresponding values were obtained using HSC Chemistry software 6.1, except for the $SmCl_3$ data which were extracted from the work by Scardala et al. who measured vapor pressures at temperatures between 680 and 804 °C [65].

In Fig. 7, it can be seen that the vapor pressures of the trichlorides are higher than 0.25×10^{-4} bar for temperatures higher than 850 °C. Consequently, volatilization of the chlorides is expected for these temperatures.

There are two unusual behaviors in the chlorination of oxides of group 2 reported in the literature. According to TPP diagrams of the Ce–O(Fig. 1a), the most stable oxide for this system is CeO_2 at temperatures between room temperature and 1000 °C and for $pO_2 > 10^{-15}$ atm. For that reason, it is interesting to study the reaction between this oxide and Cl_2(g). Esquivel et al. [25] investigated the chlorination of cerium dioxide by thermogravimetry. They concluded that the evolution of the chlorination reaction is given by reaction 9, followed by vaporization of $CeCl_3$ (reaction 32) for temperatures higher than 800 °C. These results are in agreement with the thermodynamical analysis (Fig. 4), where there is equilibrium between cerium dioxide and cerium chloride, and with $CeCl_3$ vapor pressure calculation (Fig. 7), $pVCeCl_3 = 4.6*10^{-6}$ bar at 800 °C.

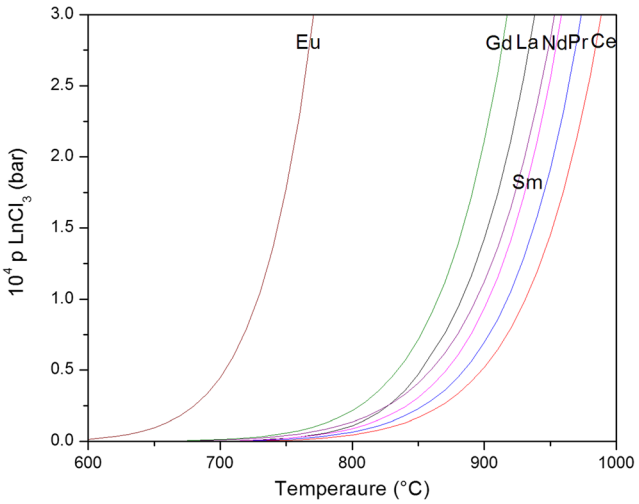

Fig. 7 Vapor pressure of $LnCl_3$

In addition to cerium, praseodymium also has different stable oxides other than sesquioxide between room temperature and 1000 °C (see Fig. 1b); Pr_6O_{11} being the most stable oxide (except for T < 500 °C and pO_2 > 1 atm). The chlorination of mixed praseodymium oxide Pr_6O_{11} with chlorine at 1 atm was investigated [23]. This reaction begins at approximately 320 °C with formation of praseodymium oxychloride. However, if it is considered that the oxychloride is PrOCl, a mass gain of ΔM/mi = 13% should be observed, and the authors obtained higher values. This behavior will be explained below in the oxychloride characterization section.

3.3 Kinetic Analyses

Reactions between gases and solids involve several complex interdependent stages such as gas phase mass transfer, diffusion of the gaseous reactant, adsorption, chemical reaction (breakage and formation of chemical bonds), diffusion of a gaseous product out of the solid particle, among others. There is vast literature on kinetic analysis of gas–solid reactions, a summary of the many quantitative and mathematical descriptions developed throughout the years, starting from the shrinking-core-based grain models [66] and the shrinking-pore-based-models [67] up to the more recent rate equations proposed is provided by Li et al. [68]. Generally, these models use different approximations such as negligible bulk flow contribution, negligible mass transfer resistance, irreversible reaction, etc. [69–71]. Another approach extensively used in gas–solid reactions are the nucleation and growth models initially developed for transformations in condensed matter [72–77]. It is well acknowledged that the chemical transformation of a solid is possible due to nucleation and growth of the product phase at the expense of the initial one. In the case of solid–gas reactions, the nuclei appear at the surface of the solid reactant phase.

If sample mass and gas flow effects are excluded, the classical rate equation of a heterogenous solid–gas reaction can be written, assuming separability of variables, as:

$$\frac{d\alpha}{\mathrm{dt}} = K(T)\cdot F(P_{\mathrm{Cl}_2})\cdot G(\alpha) \tag{33}$$

where K(T) refers to an Arrhenius type equation, $F(P_{Cl2})$ expresses the dependence of the reaction rate on the chlorine partial pressure, and G(α) is the function that describes the geometric evolution of the reacting solid.

The first condition to reach in order to carry out a kinetic study is called "chemical control of the reaction rate", in which mass transfer processes such as reaction gas starvation, diffusion through the boundary layer surrounding the solid sample, diffusion through sample pores are disregarded. For this reason, it is important to find the experimental conditions under which the reaction proceeds under chemical control. These conditions for Ln_2O_3 (Ln : La, Nd, Sm, Eu, and Gd) and Pr_6O_{11} were determined for the chlorination kinetic studies previously published [17–23].

Under "chemical control conditions," the reaction rate depends only on the intrinsic chemical reaction. The intrinsic reaction parameters: activation energy, dependence of the reaction rate on the chlorine partial pressure, and reaction mechanism were determined.

The reactions degree versus time curves obtained for these reactions have a "sigmoidal shape", which is characteristic of a process where the products are formed following a nucleation and grow mechanism. Therefore, these systems were fitted according to the Johnson–Mehl–Avrami (JMA) model according to the following equations [75, 76]:

$$\alpha = 1 - \exp(-[k(T)\cdot t]^n) \tag{34}$$

$$k(T) = k_0\cdot \exp\left(\frac{-\mathrm{Ea}}{R_g\cdot T}\right) \tag{35}$$

where *k(T)* is the global rate constant (other than *K(T)* in Eq. 33), k_0 is the pre-exponential factor, *Ea* is the effective activation energy, and *n* is the JMA exponent. Three parameters *k(T)*, *Ea*, and *n* depend on the nucleation and growth mechanisms.

Table 2 summarizes kinetic parameters published for Ln_2O_3 (Ln : La, Nd, Sm, Eu, and Gd) and Pr_6O_{11} chlorinations with chlorine and formation of lanthanide oxychlorides, determined by isothermal thermogravimetry carried out with the same reaction equipment (except for Pr_6O_{11}). It can be observed that there are not great differences between these systems; however, due to the high initial temperature of Gd_2O_3 chlorination, the chemical control was achieved at higher temperature. JMA exponents (*n*) are approximately 1.5 for all systems; this value is consistent with a three-dimensional growth and site saturation [75]. The order of partial pressure of chlorine increases with Z.

In recent years, with the use of simulation software, and powerful computational calculations, more general approches for kinetic modeling have arisen in which the rate takes the following expression [78]:

$$\frac{d\alpha}{\mathrm{dt}} = \varphi(T, P_i)\cdot S_m \tag{36}$$

where the variations of the overall rate with time are described by the S_m function (related to the model of transformation), whereas those with temperature (T) or partial pressure (P_i) are described by the $\varphi(T, P_i)$ function (reactivity of growth function), which accounts for the mechanism of growth (the elementary steps for a mechanism of growth are: adsorption/desorption, external interface reaction, internal interface reaction, diffusion of species from an interface to the other). The main advantage of this mathematical treatment is that it can be applied to processes where the rates of nucleation and growth

Table 2 Kinetic parameters for Ln_2O_3 (except Pr_6O_{11}) chlorination with Cl_2(g) and formation of lanthanide oxychloride

	La_2O_3	Pr_6O_{11}	Nd_2O_3	Sm_2O_3	Eu_2O_3	Gd_2O_3
T Chemical control	325	425	425	350	400	450
Ea (kJ mol^{-1})	113	105–123	161	130	115	132
pCl_2 order	0.23	–	0.39	–	0.54	0.77
n JMA	1.46	–	1.5–2	1.5	1.45	1.6
Ref	[17]	[23]	[18]	[19, 20]	[21]	[22]

are of the same order (they occur simultaneously) leading to a two-process kinetic model. Equation 34, on the contrary, is only applicable in the case of instantaneous nucleation and growth, or nucleation and instantaneous growth, i.e., one-process kinetic model.

With Eq. 36, kinetic models can be developed based on the choice of different physical assumptions. The corresponding $d\alpha/dt$ (or α) vs. time curves can be fitted to the experimental results using numerical opitmization procedures.

The kinetic results previously obtained for the LREE chlorinations presented in Table 2 showed no conflict with these new investigations, with the exception of Sm [22, 23]; in this case, variation of the activation energy with temperature was found. Applicability of Eq. 33 (i.e., separation of variables), should be experimentally probed to confirm the results obtained, and in case the assumption is not fulfill, application of Eq. 36 should lead to the corresponding results. However, those calculations are beyond the scope of the present work.

Finally, it is worthwhile to mention that the La_2O_3–Cl_2 system shows an unusual behavior at temperatures higher than 350 °C: the specific reaction rate increases with sample mass. This could be related to the formation of highly reactive gas intermediates such as chlorine radicals in the La_2O_3–Cl_2 interaction. These species have been reported by Pasquevich et al. [79, 80] in the carbochlorination of ZrO_2, which showed the same behavior. In the case of La, although the behavior can be explained considering formation of chlorine radicals, the presence of this species remains to be demonstrated.

4 Light Rare Earth Oxychlorides Characterization and Stability

As was explained in LREE oxides structures, the structural preferences across the lanthanide series can be explained considering lanthanide contraction. For later lanthanides that crystallize in layered SmSI and YOF structure types, the local coordination environment (hexagonally close-packed Ln and X layers with O atoms in tetrahedral holes between subsequent Ln layers) is preserved in both structures [81]. In accordance with this observation, various studies have determined the crystalline structure of LREE oxychlorides. Zachariasen in 1949 [82], and later Templeton [83] reported that LnOCl crystallizes in the tetragonal system with the Matlockite-type(PbFCl) structure (space group: P4/nmm). LnOCl structures were confirmed and analyzed by Hölsä et al. In the structure, Ln^{3+} ion bonds four oxygen and five chlorine atoms and the Ln–O (×4), Ln–Cl (×4), and Ln–Cl (×1) distances decrease linearly as a function of the Ln^{3+} ionic radius [84].

Lanthanide oxychlorides were also characterized by IR [85] and Raman [86] spectra, in these studies 15 total optical infrared fundamental modes and six Raman bands were predicted. Five peaks that are in agreement with a tetragonal structure were detected.

Due to the changes to chemical and electrical structure, corrosion resistance, and luminescence properties, among others, for different grain sizes in alloys, it is important to know the size of LnOCl produced by LREE oxides chlorination. Generally, there was an equivalence between the size of oxychlorides synthesized by reaction of Ln_2O_3 with Cl_2(g). It was observed by SEM that the oxychlorides grains are smaller than those obtained at higher temperatures (higher than $LnCl_3$ melting point); this observation agrees with the behavior expected for a nucleation and growth reaction mechanism. The average size of LnOCl produced at around 250 °C was of approximately 2 μm, whereas it was lower than 0.5 μm for chlorination at temperatures higher than 900 °C [17–23].

There are two non-stoichiometric oxychlorides reported in the literature: praseodymium and europium oxychlorides. The products of Pr_6O_{11} with Cl_2(g) at 425 °C and of Eu_2O_3 and NH_4Cl at 450 °C (crystallized at 750 °C) were characterized by different techniques (X-ray diffraction, Mössbauer spectroscopy, magnetic susceptibility measurements, and X-ray photoelectron spectroscopy). Aitasalo et al. established the presence of divalent Eu^{2+} ion as an impurity (<0.1%) in EuOCl, and this was confirmed by measurement of the paramagnetic susceptibility at low temperatures [87]. A general formula of $PrO_{1-x}Cl$ with the presence of Pr^{3+} and Pr^{4+} was proposed for the oxychlorides obtained during chlorination reactions at temperatures lower than 800 °C, being $x = 0.108$ for T = 425 °C, whereas $x = 0$ when the synthesis is carried out at 800 °C [23].

Some works have been carried out to study the stabilities of LnOCl in air. LREE oxychlorides are stable compounds in air and room temperature with the only exception being NdOCl that forms $Nd(OH)_xCl_y$ [88].

Yang et al. investigated the kinetics of dechlorination and oxidation of LREE oxychlorides under various oxygen partial pressures by non-isothermal thermogravimetry (PrOCl [89], NdOCl [90] and GdOCl [91]). The products proposed for these decompositions were PrO_2, Nd_2O_3 and Gd_2O_3. In these investigations, activation energies of 112.6, 228.3, and 137.7 kJ mol^{-1} were calculated for PrOCl, NdOCl, and GdOCl dechlorination, respectively. The decompositions begin to occur at approximately 827, 927, and 800 °C. One work [23] differs from [89], it reports that the product of PrOCl heated in air is Pr_6O_{11}.

When lanthanides oxyhalides are compared, the thermal stability of the structurally isomorphic oxyhalides decrease strongly with increasing atomic weight of the halide along the OCl > OBr > OI series, this can be correlated with the layer structure of RE oxyhalides. The lanthanides oxyiodides begin to decompose at distinctly lower temperatures (below 360 °C) than the corresponding Ln oxybromides (from 300 to 450 °C) or Ln oxychlorides (500 to 800 °C) for La–Gd oxyhalides, and Ln oxychlorides decomposition occurs in a single step to the oxides [92].

Only one work have been published about the thermal dissociation of REOCl at high temperature in vacuum (for LREEOCl between 1282 and 1411 °C) [93]. It was found that the REOCl dissociation occurs with formation of RE oxide and gaseous chloride according to the following reaction:

$$3\mathrm{REOCl(s)} = \mathrm{RE_2O_3(s)} + \mathrm{RECl_3}(g) \tag{37}$$

These reactions are not feasible to occur in a chlorination reactor because the temperature ranges of all the works analyzed in the present review are below the temperature corresponding to the beginning of REOCl thermal dissociation.

Finally, in this section, it is important to consider the stability of oxychlorides in the presence of water. REOCl was considered to be insoluble in water and does not react with water at room temperature [94].

However, in a recent work, Pan [88] published information on the reaction between rare earth oxychloride (REOCl for RE: Y, Gd, and Sm) and water in aqueous solution. Also, Lee et al. found that REOCl could react with H_2O at room temperature, forming HCl and $RE_2(OH)_5Cl{\cdot}nH_2O$ (RE : rare earths) [95].

It was found that the reactions proceed as follows:

$$5\mathrm{REOCl(s)} + 5\mathrm{H_2O(l)} = 2\mathrm{RE_2(OH)_5Cl(s)} + \mathrm{RE}^{3+}(\mathrm{aq}) + 3\mathrm{Cl}^{-}(\mathrm{aq}) \tag{38}$$

In 2019, Udayakantha published a work about functional applications of lanthanide oxyhalides [96], for this reason, this topic is not further discussed in the present review.

5 Carbochlorination

Carbochlorination is a reaction through which metallic chlorides are produced in the presence of both a reducing and chlorinating agent. Carbon [97–100] or carbon monoxide [101–104] are the most common reductants, although sulfur has been used. According to this definition, the reactions involved for simple oxides with stoichiometry M_xO_y (where M metal and O oxygen) during the carbochlorination process with solid carbon can be described by the following general equations:

$$\mathrm{M_xO_y(s)} + \mathrm{yCl_2}(g) + \mathrm{y}/2\mathrm{C(s)} = \mathrm{xMCl_{2y/x}(s,g)} + \mathrm{y}/2\mathrm{CO_2}(g) \tag{39}$$

$$\mathrm{M_xO_y(s)} + \mathrm{yCl_2}(g) + \mathrm{yC(s)} = \mathrm{xMCl_{2y/x}(s,g)} + \mathrm{yCO}(g) \tag{40}$$

Or with CO(*g*):

$$\mathrm{M_xO_y(s)} + \mathrm{yCl_2}(g) + \mathrm{yCO}(g) = \mathrm{xMCl_{2y/x}(s,g)} + \mathrm{yCO_2}(g) \tag{41}$$

With the aim of understanding the LREE oxide carbochlorination reactions, equilibrium composition plots were generated using HSC for Ln_2O_3 (Ln: La, Nd, Sm, Eu, and Gd), CeO_2, and Pr_6O_{11} carbochlorinations per mol of lanthanide considering 100% excess carbon and 100% chlorine gas and formation of only CO_2(g). These can be observed in Fig. 8. The oxides were chosen because they are the most stable at atmospheric condition according to the previous explanation. These plots complement the equilibrium compositions calculated by Anderson et al., for both cerium oxide and neodymium oxide carbochlorinations [105].

All thermodynamic analyses carried out for carbochlorination reactions are based on the Boudouard reaction:

$$\mathrm{CO_2}(g) + \mathrm{C(s)} = 2\mathrm{CO}(g) \tag{42}$$

where reaction 42 has positive values of ΔG^0 for temperatures lower than 700 °C; it is equal to zero at 700 °C, and it has negative values for temperatures above 700 °C. For this reason, it is thermodynamically expected that the chlorinations with carbon as the reducing agent occur with formation of mainly CO_2(g) for T < 700 °C, and mainly CO(g) for T > 700 °C. However, equilibrium composition curves show that the formation of both gases is possible for temperatures between 400 and 1000 °C, CO_2(g) formation prevailing for temperatures lower than 700 °C and CO(g) at higher temperatures.

The curves shown in Fig. 8 for CCl_4(g) and $COCl_2$(g), which are equal for all systems, and the data available in the

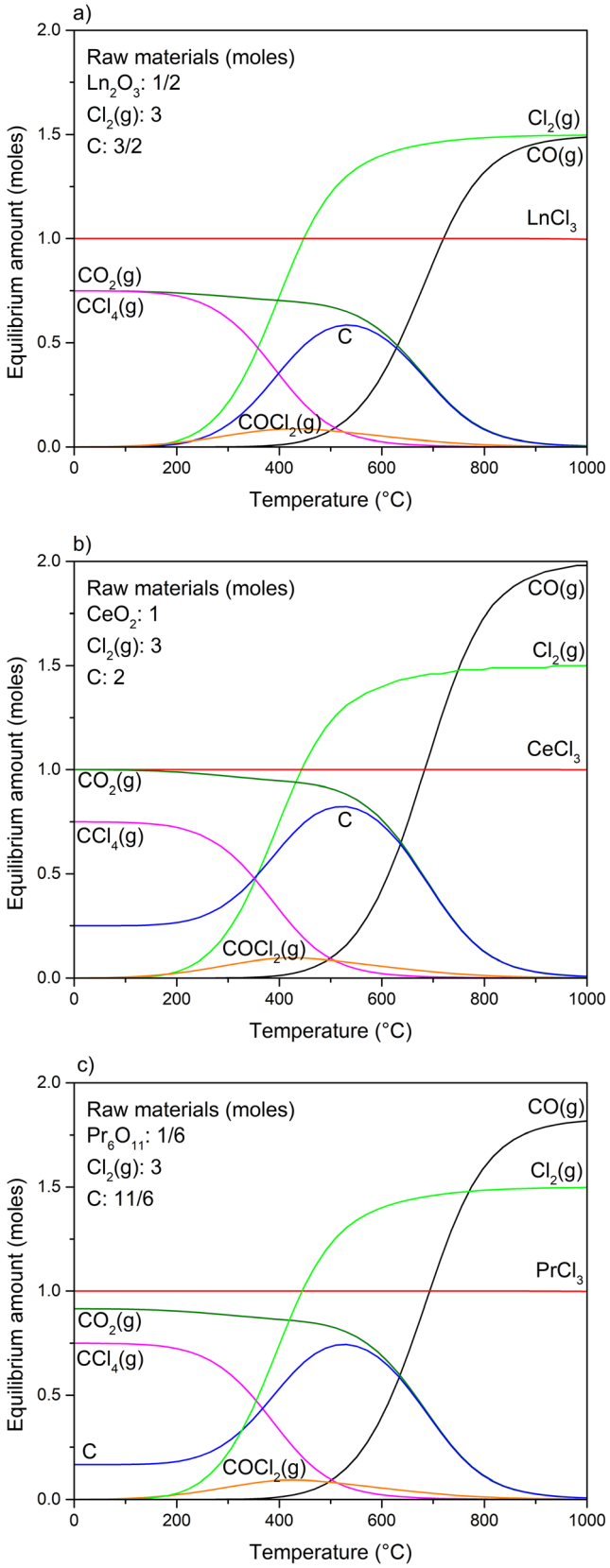

Fig. 8 Equilibrium composition plots as a function of temperature between 0 and 1000 °C according to equilibrium predictions for **a** $Ln_2O_3/C/Cl_2(g)$, **b** $CeO_2/C/Cl_2(g)$ and **c** $Pr_6O_{11}/C/Cl_2(g)$ systems

literature enable us to infer that formation of these gases is negligible for carbon in a $Cl_2(g)$–$O_2(g)$ atmosphere. The shape of $CCl_4(g)$ and $COCl_2(g)$ curves in the system suggests that these gases do not take part in the carbochlorination reaction mechanism because they are not direct reaction products, but they can be formed between gaseous species after the reaction. $CCl_4(g)$ is formed by the interaction between C and $Cl_2(g)$, and $COCl_2(g)$ can be formed by the reaction between C, $Cl_2(g)$, and $CO_2(g)$ or $Cl_2(g)$ and CO(g) [106–108].

The main difference between the systems analyzed is the concentration of $Cl_2(g)$, CO(g), $CO_2(g)$, and C. This can be understood considering the amount of oxygen in the different oxides per mol of lanthanide, having CeO_2 the highest oxygen/lanthanide relation, it can lead to the highest concentration of CO(g) and $CO_2(g)$ products which would lead to the highest consumption of $Cl_2(g)$ and C.

In agreement with that, papers have been published about carbochlorination of LREE oxides with chlorine and carbon as chlorinating and reducing agents, respectively [26–29, 105]. Anderson et al. evaluated the conversion of cerium oxide and neodymium oxide into their chlorides through the carbochlorination process, Esquivel studied the carbochlorination of CeO_2, Sm_2O_3 and its mixture, and the authors of the present article studied the carbochlorination of Eu_2O_3. Also, we studied the carbochlorination of Gd_2O_3 by infrared spectroscopy using a non-isothermal reaction system described by Guibaldo et al. [109] to determine the reaction stages and initial temperatures for each stage.

The first stage of the reaction between Ln_2O_3 (Ln: Nd, Sm, Eu, Gd), C, and $Cl_2(g)$ produced solid oxychloride. These reactions occur at temperatures comparable to those at which chlorination takes place; for example, for Eu_2O_3, the same conversion curves were determined for chlorination and carbochlorination reactions with formation of EuOCl for temperatures between 250 and 500 °C. This observation suggests that carbon is not influencing the reaction in the first stage, which is expectable taking into account the temperature of carbon oxidation in the presence of chlorine. Gonzalez et al. [110] studied the oxidation of carbons in the presence of chlorine and observed that at temperatures higher than 590, 650, and 770 °C it is possible for sucrose carbon, carbon black, and graphite, respectively, to occur. Also, chlorine chemisorption occurs at temperatures above 400 °C.

In the second stage of carbochlorination reactions, the presence of carbon allows producing trichloride at lower temperatures where this product is not volatilized. Therefore, during the REE oxide carbochlorinations, it is possible for solid REE trichlorides to be produced. The interaction between carbon and oxygen from the LREE oxide can produce both $CO_2(g)$ and CO(g) gases. The quantification of these gases is important to optimize the carbon consumption and to produce carbon-free trichlorides [11, 109, 111].

For CeO_2 carbochlorination, an initial temperature of 700 °C was determined, which is lower than the initial temperature of chlorination without carbon (800 °C). The proposed reaction products are $CeCl_3$ and CO(g), and the volatilization of the chloride is possible for T > 816 °C according to reaction 32 [27]. The phase stability diagrams for the Ce–O–Cl system (Fig. 4) showed that there is a direct boundary between the CeO_2 and the $CeCl_3$ within the reasonable operating range without formation of an intermediate phase. This would explain why the cerium oxychloride phase was not detected as an intermediate product in CeO_2 carbochlorination experiments contrary to that observed during other LREE oxides carbochlorinations. One work [105] differs from [27]; it reported that small quantities of cerium oxychloride can be formed as an intermediate product in CeO_2 carbochlorination.

By non-isothermal infrared measurements, the initial temperature of Gd_2O_3 carbochlorination was determined to be approximately 340 °C for the first stage with formation of GdOCl and approximately 600 °C for the second stage with formation of $GdCl_3$. CO_2(g) and CO(g) both are formed during oxychloride carbochlorination, and this result agrees with the observations in Y_2O_3 and YPO_4 carbochlorination [11, 30, 31]. As was explained in equilibrium composition curves, $COCl_2$(g) and CCl_4(g) were detected during the chlorination reaction due to the interaction between CO_2(g), C, and Cl_2(g).

The analysis of LREE oxide carbochlorinations suggests that the rate of the first stage is not influenced by carbon, and it is controlled by temperature and not by gas availability when there is excess carbon and chlorine gas at low temperatures. The rate values are comparable with those of the chlorination reaction. On the other hand, the rate of lanthanide chloride conversion with formation of CO(g) and CO_2(g) in the second stage is much faster than that of the chlorination reaction, and the final degree of reaction is also influenced by carbon.

Several authors have discussed the generation of reactive species during the interaction between solid carbon and gaseous chlorine. According to their works, three intermediates, Cl radicals, C–Cl compounds, and C–O–Cl compounds, should be considered in LREE oxides carbochlorinations with formation of $LnCl_3$. During interactions between gaseous chlorine and carbon surface physical and chemical adsorption phenomena can take place. These interactions involve substitution reactions in active sites, addition reactions in non-conjugated double bonds, and formation of HCl(g). The concentration of atomic chlorine according to thermodynamic considerations would be significant only at temperatures higher than 1000 °C. However, the situation is different in the presence of solid carbon because there is a heterogeneous reaction taking place, and the formation of this intermediate species would be possible during carbochlorination reactions [110, 112, 113]. Moreover, if formation of these intermediates is the rate-determining process, it is expected that the carbochlorination reactions of REE oxides with formation of $LnCl_3$ (carbon affecting the second stage) will begin at the same temperature. This in fact was observed in carbochlorination reactions for SmOCl, EuOCl, GdOCl, and YOCl, which are comparable because they were measured with the same system, and all begin at approximately 600 °C [26, 28, 30]. It should be noted that this temperature matches with the initial temperature of carbon oxidation in chlorine–oxygen atmospheres observed by Gonzalez et al. [110].

6 Applications of the LREE Chlorination and Carbochlorination Reactions

The chlorination reactions can produce LREE oxychlorides at reasonable lower temperatures (<400–500 °C) with a high reaction rate (in a laboratory scale). The oxychlorides have, at least, the same purity as the starting oxides. If the starting oxides have impurities that can be volatilized during formation of volatile chlorides, the purity of the oxychlorides will be higher than that of the initial oxides. The key for this behavior is the nature of the impurities, being possible to occur when the impurities form volatile chlorides, for example, Fe, Al, Si, or Ti. Ilmenite ($FeTiO_3$), which is found in igneous rocks, represents an important impurity in REE ores such as monazites [114]. At low temperature chlorination, impurities do not react or react very slowly, 600 °C being the initial chlorination temperature in the laboratory scale using Cl_2(g) as the chlorinating agent for $FeTiO_3$. Also, iron chlorides $FeCl_3$ and $FeCl_2$ begin to vaporize around 425 and 670 °C, respectively, whereas $CaCl_2$ vaporizes at approximately 2250 °C, and other impurities remain as solids after chlorination (SiO_2 and Al_2O_3) [115, 116]. This behavior allows LREE selective chlorinations, decreases chlorine consumption and waste generation, and allows the smallest chlorination reactors, where LREE oxides are chlorinated at lower temperatures than the impurities. For this reason, the chlorination technology for LREE processing is more efficient, sustainable, and environmentally friendly.

The REE ores are treated with chlorine gas at high temperature in the presence of reducting agents to produce REE chlorides. The main REE minerals are bastnaesite [(Ce,La)(CO_3)F], monazite [(Ce,La)PO_4)], xenotime (YPO_4), loparite [(Ce,Na,Ca)(Ti,Nb)O_3], apatite [(Ca,REE,Sr,Na,K)$_3$$Ca_2$($PO_4$)$_3$(F,OH)], and ion-adsorption clays, and 95% of the world's reserves of REEs are bastnasite (70–75% REEO), monazite (55–60% REEO), and xenotime (55–60% REEO) [2, 117].

Carbochlorination reactions can be used for element separation or for $LREECl_3$ production. The first application is based on the different chloride vaporization temperatures. If the carbochlorination is used for $LREECl_3$ production, it is important to use less than the stoichiometric amount of carbon

in order to obtain a carbon-free chloride. Contrary to LREE oxychlorides, the trichlorides are highly hygroscopic. The interaction of the trichlorides with air humidity can produce crystalline compounds of the $LREECl_3.nH_2O$ type. It is not easy to remove the water and recuperate the anhydrous trichloride (readily tends to form the oxychloride). This behavior is an advantage of the carbochlorination against the wet methods for the production of anhydrous $LREECl_3$. The carbochlorination was used to obtain REE chloride from ores such as monazite, mixed bastnaesite-monazite and xenotime [11, 32, 118]. Adachi and their collaborators studied a combined method of chlorination or carbochlorination followed by chemical vapor transport to recover REE from different materials such as those used for polishes and scrap [12, 119].

The first step in the chlorination or carbochlorination process is to grind the ore and then mix it with a binder and some water. The most common binders used are sulfite liquor, sugar, and starch. The ore mixture is then compacted into pellets through a briquetting machine. The pellets and loose layers of carbon are then placed in a chlorination furnace. The furnace is lined with carbon and designed to run at temperatures of 1000–1200 °C. The temperature required for producing from silicate or phosphate ores was found to be higher than when processing oxide ores [2, 15].

Finally, on an industrial scale, the Goldschmidt process is a high temperature direct chlorination process that has been used on a production scale at Th. Goldschmidt AG located in Germany. This process was developed to produce anhydrous rare earth chlorides directly from bastnaesite ore. This process has also been proven to be effective for other rare earth ores such as monazite or xenotime as well as for rare earth oxide concentrates [8]. REE ore is obtained from mining on the Kola Peninsula, Russia, which is refined by Solikamsk Magnesium Works (SMW) to produce REE chlorides, the REE ores are chlorinated with chlorine gas at high temperatures with reducing agents such as carbon to produce REE chlorides [120]. In China, Baotau concentrates (mainly bastnaesite and monazite) have been directly chlorinated in the presence of carbon at high temperature (1000 °C) with a recovery rate of REE of 91%. Bastnaesite beneficiated using chlorine has higher recovery yield (91–97%) and a lower energy consumption than using sulfuric acid (with 72% recovery yield and higher energy consumption), especially because for chlorination processes, the roasting of the concentrate is not required. The reaction between bastnaesite and $Cl_2(g)$ is:

$$3(Ce,La)(CO_3)F + 3Cl_2(g) = (Ce,La)F_3 + 2(Ce,La)Cl_3 + 3/2O_2(g) + 3CO_2(g) \quad (43)$$

However, the main inconvenience of the bastnaesite chlorination is the generation of high fluorine content and radioactive thorium contamination in the RE chlorides products [2, 121–123].

Due to this problem, Bargeron and collaborators proposed in a patent the addition of a boron-containing Lewis acid acting as a defluorination agent to optimize the production of REE chlorides by the dry carbochlorination method with $Cl_2(g)$ of REE concentrate (approx. 20% of RE). The boron containing Lewis acid comprises at least one of $B(OH)_3$, BCl_3, B_2O_3, $Na_2B_4O_7$ or mixtures thereof, and for $BCl_3(g)$, the ratio of $Cl_2(g)/BCl_3(g)$ ranges between approximately 1 and 20 depending on the reactive gas used. In this study, the temperature was optimized to eliminate the uranium and throrium contamination, and an elimination of approximately 50% of uranium and thorium chlorides was determined in the gaseous product of the chlorination reactor for reaction temperatures between 800 and 900 °C. Subsequently, uranium and thorium chlorides could be condensed and recovered in a condenser at temperatures between 200 and 700 °C [124].

In India, Indian Rare Earths Limited (IREL) and Kerala Minerals and Metals Limited are engaged in mining and processing beach sand minerals from placer deposits. IREL produced 22 tons of rare earths, namely RE fluoride, cerium oxide, and cerium hydrate from conversion of RE chloride in 2008–09 [125].

7 Conclusions

Studies of light rare earth oxides chlorination using chlorine as the chlorinating agent have been summarized systematically; the thermodynamics, mechanisms, and kinetics of these reactions were presented and analyzed. In the present article, lanthanides between lanthanum to gadolinium were considered as LREE, and this subdivision has been discussed in the literature; some behaviors of gadolinium, such as initial temperature of Gd_2O_3 chlorination and some thermodynamic observations, place this element intermediate between light and heavy rare earth. In this study, first, LREE are analyzed according to the possible oxidation states that the lanthanides can acquire, they are divided into three groups: La and Gd (3+ as the only possible oxidation state), Ce and Pr (they can present the 3+ oxidation state in addition to 4+), and Nd, Sm, and Eu (with 2+ and 3+ possible oxidation states). The published experimental results about reactions between LREE oxides with $Cl_2(g)$ were analyzed and also the presence of carbon as the reducing agent was considered. Reactions between LREE oxides and chlorine have been investigated using mainly thermogravimetry. In all those investigations, it was determined that the reactions begin at approximately 250 °C, except for Gd_2O_3 that begins at 327 °C.

The kinetics of the chlorination of LREE oxides was reviewed in the light of recently developed kinetic approaches. It was concluded that the intrinsic kinetic

parameters of the reaction rates already published are consistent with new research. Unusual behaviors observed in the chlorination of samarium and lanthanum oxides may leave room for some extra investigations. Comparing the intrinsic kinetic parameters obtained for the different systems, it was found that activation energies are between 105 and 161 kJ mol^{-1}; Pr_6O_{11} and Nd_2O_3 being the oxides with lowest and highest values, respectively. The order with respect to $Cl_2(g)$ partial pressure is between 0.23 and 0.77 and increases with the atomic number. Finally, the JMA n-value is approximately 1.5 for all the oxide chlorinations.

The similarities and differences among elements of the LREE group detailed in this review could be further analyzed using computational simulation techniques. However, that would be the subject of a future investigation.

This review includes a special section about the characterization and stability of LREE oxychlorides. Structural preferences of lanthanide oxychlorides come in large measure from the relative ratio of the ionic radii and the strengths of electrostatic interactions. As such, the crystal structures adopted by LnOCl compounds can be described by a tetragonal system with the Matlockite-type(PbFCl) structure. Studies regarding the stability of LREE oxychlorides under different atmospheres were analyzed, and development of this area of research is imperative for different applications of these compounds. For the same reason, it is important to gain knowledge about the behavior of LnOCl in air (or oxygen at different partial pressure), vacuum, inert gases, and water at different temperatures.

For Ln_2O_3 carbochlorinations, two stages were determined. The first stage proceeds with formation of solid oxychloride. These reactions occur at temperatures comparable to those of chlorination reactions, suggesting that carbon is not influencing in the first stage. Whereas the second stage, in which $LnCl_3$, $CO_2(g)$, and CO(g) are produced, is influenced by carbon, and this reaction is much faster than the chlorination reaction without a reducing agent. Furthermore, the reactions begin at the same temperature (approx. 600 °C), and this temperature also corresponds to the initial temperature for carbon oxidation in chlorine–oxygen atmospheres, independently of LREE. These observations could indicate that the rate-determining process is equal for all analyzed systems, and according to literature, this step involves the formation of intermediates such as Cl radicals, C–Cl compounds, and C–O–Cl compounds.

Another aspect that has been included in this work considers chlorination and carbochlorination reactions of LREE compounds, such as oxides and ores. Chlorination is a very effective metallurgical method to treat various kinds of complex LREE ore resources. The most studied ores were bastnaesite and monazite, which were chlorinated both at a laboratory and industrial scale using $Cl_2(g)$ and carbon to obtain LREE chlorides. It is necessary to consider different advantages and disadvantages of chlorination methods and to improve their benefits in the development of LREE recovery processes. For instance, the generation of high fluorine content and radioactive thorium contamination, diminution of $Cl_2(g)$ and carbon consumption, reaction temperature optimization, among others.

Acknowledgments The financial support from Comisión Nacional de Energía Atómica (CNEA), Consejo Nacional de Investigaciones Científicas y Técnicas (CONICET), and Ministerio de Ciencia, Tecnología e Innovación Productiva, Agencia Nacional de Promoción Científica y Tecnológica (ANPCyT) is gratefully acknowledged.

References

1. Connelly NG, Damhus T, Hartshorn RM, Hutton AT (eds) (2005) Nomenclature of inorganic chemistry: IUPAC recommendations. Royal Society of Chemistry, London, pp 51
2. Gupta CK, Krishnamurthy N (2005) Extractive metallurgy of rare earths. CRC, London, pp 27–31; 151–2
3. Shannon RD (1976) Revised effective ionic radii studies of interatomic distances in halides and chalcogenides. Acta Cryst A32: 751–767. https://doi.org/10.1107/S0567739476001551
4. Cotton S (2020) Two centuries of the rare earths. Chimie nouvelle N° 133, pp 1–12
5. Goodenough KM, Wall F, Merriman D (2018) The rare earth elements: demand, global resources, and challenges for resourcing future generations. Nat Resour Res 27(2):201–216. https://doi.org/10.1007/s11053-017-9336-5
6. Zhou B, Li Z, Chen C (2017) Global potential of rare earth resources and rare earth demand from clean technologies. Minerals 7(11):203. https://doi.org/10.3390/min7110203
7. Okabe P, Newton M, Rappleye D, Simpson MF (2020)Gas-solid reaction pathway for chlorination of rare earth and actinide metals using hydrogen and chlorine gas. J Nucl Mater 534:152156. https://doi.org/10.1016/j.jnucmat.2020.152156
8. Habashi F (1997) Handbook of extractive metallurgy, vol 3. Wiley-VCH, Weinheim
9. Möller P, Cerný P, Saupé F (1989) Lanthanides, tantalum and niobium, proceedings of the workshop in Berlin, November 1986. Springer, Berlin Heidelberg, pp 349–351
10. Jena PK, Brocchi EA (1997) Metal extraction through chlorine metallurgy. Miner Process Extr Metall Rev 16(4):211–237. https://doi.org/10.1080/08827509708914136
11. Wang Z, Zhang L, Lei P, Chi M (2002) Rare earth extraction and separation from mixed bastnaesite-monazite concentrate by stepwise carbochlorination–chemical vapor transport. Metall Mater Trans B Process Metall Mater Process Sci 33B:661–668. https://doi.org/10.1007/s11663-002-0018-1
12. Adachi G, Shinozaki K, Hirashima Y, Machida K (1991) Rare earth separation using chemical vapor transport with LnCl,-AlCl, gas phase complexes. J Less Common Met 169:L1–L4. https://doi.org/10.1016/0022-5088(91)90225-S
13. Jiang J, Ozaki T, Machida K, Adachi G (1997) Separation and recovery of rare earths via a dry chemical vapour transport based on halide gaseous complexes. J Alloys Compd 260:222–235. https://doi.org/10.1016/S0925-8388(97)00176-X
14. Murase K, Machida K, Adachi G (1994) Vapor phase extraction and mutual separation of rare earths from monazite using chemical vapor transport mediated by vapor complexes. Chem Lett 23(7): 1297–1300. https://doi.org/10.1246/cl.1994.1297

15. Binnemans K, Jones PT, Blanpain B, Van Gerven T, Yang Y, Walton A, Buchert M (2013) Recycling of rare earths: a critical review. J Clean Prod 51:1–22. https://doi.org/10.1016/j.jclepro.2012.12.037
16. Kaplan V, Wachtel E, Gartsman K, Feldman Y, Park K, Lubomirsky I (2021) Using chlorine gas to recover rare earth metals from end-of-life permanent magnets. JOM 73:1957–1965. https://doi.org/10.1007/s11837-021-04592-3
17. Gaviría JP, Navarro LG, Bohé AE (2012) Chlorination of lanthanum oxide. J Phys Chem A 116(9):2062–2070. https://doi.org/10.1021/jp210457r
18. Bosco MV, Fouga GG, Bohé AE (2012) Kinetic study of neodymium oxide chlorination. Thermoch Acta 540:98–106. https://doi.org/10.1016/j.tca.2012.04.014
19. Esquivel MR, Bohé AE, Pasquevich DM (2005) Chlorination of Sm_2O_3. J Mater Process Technol 170:304–309
20. Esquivel MR, Bohé AE, Pasquevich DM (2005) A quantitative analysis of the chlorination of samarium sesquioxide. Mater Sci Eng A 397:310–313. https://doi.org/10.1016/j.msea.2005.02.061
21. Pomiro FJ, Fouga GG, Bohé AE (2013) Kinetic study of europium oxide chlorination. Metall Mater Trans B Process Metall Mater Process Sci 44:1509–1519. https://doi.org/10.1007/s11663-013-9931-8
22. Pomiro FJ, Fouga GG, Gaviría JP, Bohé AE (2015) Thermogravimetry study of Gd_2O_3 chlorination. Kinetics and characterization of gadolinium oxychloride. J Therm Anal Calorim 122(2):679–687. https://doi.org/10.1007/s10973-015-4738-2
23. Pomiro FJ, Gaviría JP, Fouga GG, Vega LD, Bohé AE (2019) Chlorination of Pr_2O_3 and Pr_6O_{11}. Crystal structure, magnetic and spectroscopic properties of praseodymium oxychloride. J Alloys Compd 776:919–926. https://doi.org/10.1016/j.jallcom.2018.10.329
24. Gaviría JP, Bohé AE (2009) The kinetics of the chlorination of yttrium oxide. Metall Trans B 40:45–53. https://doi.org/10.1007/s11663-008-9215-x
25. Esquivel MR, Bohé AE, Pasquevich DM (2003) Chlorination of cerium dioxide. Thermoch Acta 398:81–91. https://doi.org/10.1016/S0040-6031(02)00323-4
26. Pomiro FJ, Fouga GG, Gaviría JP, Bohé AE (2014) Study of the reaction stages and kinetics of the europium oxide carbochlorination. Metall Mater Trans B Process Metall Mater Process Sci 46(1):304–315. https://doi.org/10.1007/s11663-014-0196-7
27. Esquivel MR, Bohé AE, Pasquevich DM (2002) Carbochlorination of cerium dioxide. Trans Inst min Metall (sect. C: mineral process Extr Metall) 111/proc. Australas. Inst Min Metall 307:C149–C155. https://doi.org/10.1179/037195502766647075
28. Esquivel MR, Bohé AE, Pasquevich DM (2003) Carbochlorination of samarium sesquioxide. Thermoch Acta 403:207–218. https://doi.org/10.1016/j.jmatprotec.2005.05.007
29. Esquivel MR, Bohé AE, Pasquevich DM (2005) Effect of reaction temperature on the chlorination of a Sm_2O_3–CeO_2–C mixture. Thermoch Acta 432:47–55. https://doi.org/10.1016/j.tca.2005.04.011
30. Gaviría JP, Bohé AE (2010) Carbochlorination of yttrium oxide. Thermoch Acta 509:100–110. https://doi.org/10.1016/j.tca.2010.06.009
31. Gaviría JP, Fouga GG, Bohé AE (2011) Kinetics of yttrium oxide carbochlorination. Thermoch Acta 517:24–33. https://doi.org/10.1016/j.tca.2011.01.026
32. Gimenes MA, Oliveira HP (2001) Microstructural studies and Carbochlorination kinetics of Xenotime ore. Metall Mater Trans B Process Metall Mater Process Sci 32B:1007–1013. https://doi.org/10.1007/s11663-001-0089-4
33. Murase K, Ozaki T, Machida K, Adachi G (1996) Extraction and mutual separation of rare earths from concentrates and crude oxides using chemical vapor transport. J Alloys Compd 233:96–106. https://doi.org/10.1016/0925-8388(96)80040-5
34. Braginski AI, Isenberg AO, Miller MT, Oeffinger TR (1972) Chlorination of yttrium oxide in presence of carbon. Ceramic Bulletin 51(8):630–632 636
35. Brugger W, Greinacher E (1967) A process for direct chlorination of rare earth ores at high temperatures on a production scale. JOM 19:32–35. https://doi.org/10.1007/BF03378662
36. Zimmerman JB, Ingles JC (1960) Isolation of the rare earth elements. Anal Chem 32(2):241–246
37. Zhang LQ, Zhang FC, Yao SH, Jiang LL, Wang XH (2007) Rare earth extraction from mixed bastnaesite-monazite concentrate by carbochlorination-oxidation. Chin J Process Eng 7(1):75–78. https://doi.org/10.3321/j.issn:1009-606X.2007.01.016
38. Augusto EB, Oliveira HP (2001) Kinetics of chlorination and microstructural changes of Xenotime by carbon tetrachloride. Metall Trans B 32:783–791. https://doi.org/10.1007/s11663-001-0065-z
39. Miller JF, Miller SE, Himes RC (1959) Preparation of anhydrous rare earth chlorides for physicochemical studies. J Am Chem Soc 81:4449–4451. https://doi.org/10.1021/ja01526a003
40. Ozaki T, Murase K, Machida KI, Adachi GY (1996) Extraction of rare earths and thorium from monazite by chlorination with carbon tetrachloride. Trans Instn Min Metall (Sect C: Mineral Process Extr Metall) 105:141–145
41. Iordanov N, Daiev K (1962) Separation of small amounts of the rare earths from minerals and rocks by chlorination with carbon tetrachloride. Zh Anal Khim 17(4):429–431
42. Itoh M, Miura K, Machida K (2009) Novel rare earth recovery process on Nd–Fe–B magnet scrap by selective chlorination using NH_4Cl. J Alloys Compd 477:484–487. https://doi.org/10.1016/j.jallcom.2008.10.036
43. Gaede DW, Ruffier BD, Downey JP, Chorney JL, Twidwell LG, Foy RJ, Lyons KM (2015) Chlorination roasting of rare earth element oxides, drying, roasting, and calcining of minerals. Springer, Cham, pp 11–18. https://doi.org/10.1007/978-3-319-48245-3_2
44. Zhu GC, Chi RA, Zhang ZG (2000) Chlorinating mechanism of cerium dioxide by NH_4Cl. J Chin Rare Earth Soc 18(4):293–296. https://doi.org/10.3321/j.issn:1000-4343.2000.04.002
45. Zhu G, Chi R, Shi W (2003) Chlorination kinetics of fluorine-fixed rare earth concentrate. Miner Eng 16(7):671–674. https://doi.org/10.1016/S0892-6875(03)00129-8
46. Zhu GC, Chi RA (2006) Kinetics of chlorinating rare earth in bastnaesite with NH4Cl chlorinating method after fixed fluorine treatment. Chin Rare Earths 27(1):65–69. https://doi.org/10.3969/j.issn.1004-0277.2006.01.019
47. Shi WZ, Zhu GC, Hua J (2003) Recovery of RE from Baotou rare earth concentrate with chlorination roasting. Trans Nonferrous Metals Soc China 13(2):438–442
48. Shi WZ, Zhang X, Zhu GC (2004) Kinetics in chlorinating mixed rare earth oxides reaction process by ammonium chloride. Chin J Rare Met 28(6):1019–1023. https://doi.org/10.3969/j.issn.0258-7076.2004.06.014
49. Shi WZ, Zhang X, Zhao YH (2005) Kinetics on chlorination process of La_2O_3 and CeO_2 by ammonium chloride. Chin J Process Eng 5(1):23–28. https://doi.org/10.3321/j.issn:1009-606X.2005.01.005
50. Chen HN, Sun YH, Fu YX (2008) Direct preparation of anhydrous lanthanide chlorides from lanthanide oxides chlorinated by NH_4Cl. Chin Rare Earths 29(2):54–59. https://doi.org/10.16533/j.cnki.15-1099/tf.2008.02.009

51. Chu YX, Shi WZ, Zuo CS (2016) Chlorination of Sm_2O_3(s) with NH_4Cl(s) roasting method and its kinetics. Henan Sci 11:1808–1811
52. Lorenz T, Bertau M (2017) Recycling of rare earth elements. Phys Sci Rev 2(1). https://doi.org/10.1515/psr-2016-0067
53. Lorenz T, Bertau M (2019) Recycling of rare earth elements from FeNdB-magnets via solid-state chlorination. J Clean Prod 215: 131–143. https://doi.org/10.1016/j.jclepro.2019.01.051
54. Lim KH, Choi CU, Moon G, Lee T, Kang J (2021) Selective chlorination of rare earth elements from a Nd-Fe-B magnet using zinc chloride. J Sustain Metall 7:794–805. https://doi.org/10.1007/s40831-021-00380-0
55. Xing Z, Cheng G, Yang H, Xue X, Jiang P (2020) Mechanism and application of the ore with chlorination treatment: a review. Miner Eng 154:106404. https://doi.org/10.1016/j.mineng.2020.106404
56. Cotton S (2006) Lanthanide and actinide chemistry. Wiley, New York
57. Outotec research oy (2007) HSC Chemistry software version 6.12. Outotec research oy, Pori, Finland
58. Jacob KT, Dixit A, Rajput A (2016) Stability field diagrams for ln–O–cl systems. Bull Mater Sci 39(3):603–611. https://doi.org/10.1007/s12034-016-1219-6
59. Brown D (1968) Halides of the lanthanides and actinides. Wiley, London
60. Haschke JM (1979) Halides, handbook on the physics and chemistry of rare earths, Vol 4, Chap 32. North-Holland, Amsterdam
61. Haibel E, Füglein E, Schulze AS, Walter D (2019) Thermal decomposition of carbonated lanthanum hydroxide. J Therm Anal Calorim 138:3571–3575. https://doi.org/10.1007/s10973-019-08461-9
62. Atkinson SC (2014) Crystal structures and phase transitions in the rare earth oxides. PhD Thesis, University of Salford
63. Zinkevich M (2007) Thermodynamics of rare earth sesquioxides. Prog Mater Sci 52:597–647. https://doi.org/10.1016/j.pmatsci.2006.09.002
64. De Micco G, Pasquevich DM, Bohé AE (2007) Chlorination of aluminium–copper alloys. Thermoch Acta 457:83–91. https://doi.org/10.1016/j.tca.2007.02.012
65. Scardala P, Villani AR, Brunetti B, Piacente V (2003) Vaporization study of samarium trichloride, samarium tribromide and samarium diiodide. Mater Chem Phys 78:637–644. https://doi.org/10.1016/S0254-0584(02)00190-6
66. Szekely J, Evans JW, Sohn HY (1976)Gas-solid reactions. Academic, New York
67. Peterson EE (1957) Reaction of porous solids. AICHE J 3(4):443–448. https://doi.org/10.1002/aic.690030405
68. Li Z (2020) General rate equation theory for gas–solid reaction kinetics and its application to CaO carbonation. Chem Eng Sci 227:115902. https://doi.org/10.1016/j.ces.2020.115902
69. Sohn HY (2019) Review of fluid-solid reaction analysis—part 1: single nonporous reactant solid. Can J Chem Eng 97(7):2061–2067. https://doi.org/10.1002/cjce.23469
70. Sohn HY (2019) Review of fluid-solid reaction analysis—part 2: single porous reactant solid. Can J Chem Eng 97(7):2068–2076. https://doi.org/10.1002/cjce.23468
71. Pijolat M, Favergeon L (2018) Chapter 5 - kinetics and mechanisms of solid-gas reactions. Handbook of thermal analysis and calorimetry. Elsevier, Amsterdam, Vol 6, pp 173–212
72. Avrami M (1939) Kinetics of phase change. I general theory. J Chem Phys 7(12):1103–1113. https://doi.org/10.1063/1.1750380
73. Avrami M (1940) Kinetics of phase change. II transformation: time relations for random distribution of nuclei. J Chem Phys 8(2):212–224. https://doi.org/10.1063/1.1750631
74. Avrami M (1941) Granulation, phase change, and microstructure kinetics of phase change. III. J Chem Phys 9(2):177–184. https://doi.org/10.1063/1.1750872
75. Kempen ATW, Sommer F, Mittemeijer EJ (2002) Determination and interpretation of isothermal and non-isothermal transformation kinetics; the effective activation energies in terms of nucleation and growth. J Mater Sci 37(2):1321–1332. https://doi.org/10.1023/A:1014556109351
76. Johnson WA, Mehl RF (1939) Reaction kinetics in processes of nucleation and growth. Trans Am Inst Min Metall Engs 135:416–427
77. Barmak KN (2018) A commentary on: "reaction kinetics in processes of nucleation and growth". Metall Mater Trans B Process Metall Mater Process Sci 49:3616–3680. https://doi.org/10.1007/s11663-010-9421-1
78. Pijolat M, Favergeon L, Soustelle M (2011) From the drawbacks of the Arrhenius-f(α) rate equation towards a more general formalism and new models for the kinetic analysis of solid–gas reactions. Thermoch Acta 525(1–2):93–102. https://doi.org/10.1016/j.tca.2011.07.026
79. Pasquevich DM (1990) PhD Thesis, Facultad de Ciencias Exactas de la Universidad Nacional de La Plata, La Plata, Argentina
80. Pasquevich DM, Amorebieta VT (1992) Mass spectrometric study of volatile products during the carbochlorination of zirconia. V Ber Bunsen-Ges Phys Chem 96(4):534–541. https://doi.org/10.1002/bbpc.19920960403
81. Garcia E, Corbett JD, Ford JE, Vary WJ (1985)Low-temperature routes to new structures for yttrium, holmium, erbium, and thulium oxychlorides. Inorg Chem 24(4):494–498. https://doi.org/10.1021/ic00198a013
82. Zachariasen WH (1949) Crystal chemical studies of the 5f-series of elements. XII. New compounds representing known structure types. Acta Cryst 2:388–390. https://doi.org/10.1107/S0365110X49001016
83. Templeton DH, Dauben CH (1953) Crystal structures of rare earth oxychlorides. J Am Chem Soc 75(23):6069–6070. https://doi.org/10.1021/ja01119a535
84. Hölsä J, Lahtinen M, Lastusaari M, Valkonen J, Viljanen J (2002) Stability of rare-earth oxychloride phases: bond valence study. J Solid State Chem 165(1):48–55. https://doi.org/10.1006/jssc.2001.9491
85. Basile LJ, Ferraro JR, Gronert D (1971) I.R. spectra of several lanthanide oxyhalides. J Inorg Nucl Chem 33:1047–1053. https://doi.org/10.1016/0022-1902(71)80173-2
86. Del Cul GD, Nave SE, Begun GM, Peterson JR (1992) Raman spectra of tetragonal lanthanide oxychlorides obtained from polycrystalline and single-crystal samples. J Raman Spectrosc 23:267–272. https://doi.org/10.1002/jrs.1250230505
87. Aitasalo T, Holsa J, Lastusaari M, Legendziewicz J, Lehto L, Linden J, Marysko M (2004) Structural, magnetic and spectroscopic investigations of europium oxychloride, EuOCl. J Alloys Compd 380:296–302. https://doi.org/10.1016/j.jallcom.2004.03.057
88. Pan B, Zhang Z, Lu X (2020) Determination and application of the reaction between REOCl (RE = Y, Gd and Sm) and H_2O. Chem Pap 74:3987–3993. https://doi.org/10.1007/s11696-020-01202-5
89. Yang HC, Eun HC, Cho YZ, Lee HS, Kim IT (2009) Kinetic analysis of dechlorination and oxidation of PrOCl by using a non-isothermal TG method. Thermoch Acta 484:77–81. https://doi.org/10.1016/j.tca.2008.11.012
90. Yang HC, Cho YJ, Eun HC, Kim EH, Kim IT (2007) Kinetic study of a thermal dechlorination and oxidation of neodymium oxychloride. Thermoch Acta 460:53–59. https://doi.org/10.1016/j.tca.2007.05.019
91. Yang HC, Cho YJ, Eun HC, Kim EH, Kim IT (2007) Kinetic analysis of a thermal Dechlorination and oxidation of gadolinium oxychloride. J Therm Anal Calorim 90:379–384. https://doi.org/10.1007/s10973-006-7947-x

92. Hölsä JPK (1982) Thermal stabilities of selected rare earth oxyiodides. J Therm Anal 25:127–133. https://doi.org/10.1007/BF01913061
93. Patrikeev YB, Novikov GI, Badovskii VV (1973) Thermal dissociation of scandium, yttrium and lanthanum oxide chlorides. Russ J Phys Chem 47:284
94. Lee SS, Park HI, Joh CH, Byeon SH (2007)Morphology-dependent photoluminescence property of red-emitting LnOCl:Eu (ln = La and Gd). J Solid State Chem 180(12):3529–3534. https://doi.org/10.1016/j.jssc.2007.10
95. Lee BI, Jeong H, Byeon SH (2014) Oxychloride–hydroxychloride–trihydroxide phase relationships of rare earths in aqueous solution. Inorg Chem 53(10):5212–5221. https://doi.org/10.1021/ic500403v
96. Udayakantha M, Schofield P, Waetzig GR, Banerjee S (2019) A full palette: crystal chemistry, polymorphism, synthetic strategies, and functional applications of lanthanide oxyhalides. J Solid State Chem 270:569–592. https://doi.org/10.1016/j.jssc.2018.12.017
97. Wang L, Zhang TA, Lv GZ, Dou ZH, Zhang WG, Zhang JZ, Liu Y (2019) Carbochlorination of alumina and silica from high-alumina fly ash. Miner Eng 130:85–91. https://doi.org/10.1016/j.mineng.2018.09.022
98. Li Y, Duan D, Liu Y, Yang X (2017) Reaction thermodynamics of Al_2O_3, Fe_2O_3, and SiO_2 during carbochlorination. Process Chem Lett 46(5):775–777. https://doi.org/10.1246/cl.161166
99. Wang L, Zhang TA, Lv GZ, Dou ZH, Sun WH, Zhang WG, Niu LP, Zhang ZM (2019) Titanium extraction from fly ash by carbochlorination. JOM 71(12):4624–4630. https://doi.org/10.1007/s11837-019-03460-5
100. Ruiz MDC, González JA, Rivarola JB (2004) Kinetics of chlorination of tantalum pentoxide in mixture with sucrose carbon by chlorine gas. Metall Mater Trans B Process Metall Mater Process Sci 35(3):439–448. https://doi.org/10.1007/s11663-004-0045-1
101. Kim CH, Woo SI, Jeon SH (2000) Recovery of platinum-group metals from recycled automotive catalytic converters by carbochlorination. Ind Eng Chem Res 39(5):1185–1192. https://doi.org/10.1021/ie9905355
102. Shen SB, Hao XF, Yang GW (2009) Kinetics of selective removal of iron from chromite by carbochlorination in the presence of sodium chloride. J Alloys Compd 476(1–2):653–661. https://doi.org/10.1016/j.jallcom.2008.09.109
103. Kanari N, Gaballah I, Allain E (1999) A study of chromite carbochlorination kinetics. Metall Mater Trans B Process Metall Mater Process Sci 30:577–587. https://doi.org/10.1007/s11663-999-0018-5
104. Djona M, Allain E, Gaballah I (1995) Kinetics of chlorination and carbochlorination of molybdenum trioxide. Metall Mater Trans B Process Metall Mater Process Sci 26:703–710. https://doi.org/10.1007/BF02651716
105. Anderson A, Mishra B (2005) Investigation of the carbochlorination process for conversion of cerium and neodymium oxides into their chlorides. J Sustain Metall 1:189–198. https://doi.org/10.1007/s40831-015-0023-7
106. Schnöckel H, Eberlein RA, Plitt HS (1992) Infrared spectra of matrix isolated ClCO and ab initio calculation. J Chem Phys 97(4):4–7. https://doi.org/10.1063/1.463980
107. Stringer J, Banerjee DD (1991) Chlorine in coal: proceedings of an international conference, Elsevier, Amsterdam, pp 195–206
108. Yudovich YE, Ketris MP (2006) Chlorine in coal: a review. Int J Coal Geol 67(1–2):127–144. https://doi.org/10.1016/j.coal.2005.09.004
109. Guibaldo CN, Pomiro FJ, De Micco G, Bohé AE (2016) Infrared study of the carbochlorination of MoO_3 with gaseous chlorine below 703 K. Thermoch Acta 627:9–19. https://doi.org/10.1016/j.tca.2016.01.017
110. Gonzalez J, Ruiz MDC, Bohé A, Pasquevich D (1999) Oxidation of carbons in the presence of chlorine. Carbon 37(12):1979–1988. https://doi.org/10.1016/S0008-6223(99)00063-9
111. Brocchi EA, Navarro RCS, Moura FJ (2013) A chemical thermodynamics review applied to V_2O_5 chlorination. Thermoch Acta 559:1–16. https://doi.org/10.1016/j.tca.2013.01.025
112. Li Y, Duan DP, Liu Y, Yang XM (2017) Reaction thermodynamics of Al_2O_3, Fe_2O_3, and SiO_2 during carbochlorination process. Chem Lett 46(5):775–777. https://doi.org/10.1246/cl.161166
113. Pasquevich L, Gamboa J, Caneiro A (1992) On the role of carbon in the carbochlorination refractory oxides. Thermochim Acta 209:209–222. https://doi.org/10.1016/0040-6031(92)80200-G
114. Walters A, Lusty P, Hill A (eds) (2011) Rare earth elements. British Geological Survey, Nottingham
115. Rhee KI, Sohn HY (1990) The selective chlorination of iron from llmenite ore by CO-Cl_2 mixtures: part I. intrinsic kinetics. Metall Trans B 21(2):321–330. https://doi.org/10.1007/BF02664200
116. Kim J, Lee YR, Jung EJ (2021) A study on the roasting process for efficient selective chlorination of ilmenite ores. JOM 73:1495–1502. https://doi.org/10.1007/s11837-021-04620-2
117. Royen H, Fortkamp U (2016) Rare earth elements – purification, separation and recycling. IVL Swedish Environmental Research Institute, Stockholm
118. Cen P, Bian X, Liu Z, Gu M, Wu W, Li B (2021) Extraction of rare earths from bastnaesite concentrates: a critical review and perspective for the future. Miner Eng 171:107081. https://doi.org/10.1016/j.mineng.2021.107081
119. Ozaki T, Machida K, Adachi G (1999) Extraction and mutual separation of rare earths from used polishes by chemical vapor transport. Metall Mater Trans B Process Metall Mater Process Sci 30B:45–51. https://doi.org/10.1007/s11663-999-0005-x
120. Joint-Stock Company Solikamsk Magnesium Works (2016) Annual Report 2015. Solikamsk
121. Talens Peiró L, Villalba Méndez G (2013) Material and energy requirement for rare earth production. JOM 65:1327–1340. https://doi.org/10.1007/s11837-013-0719-8
122. Yang F (2012) Situation and policies for China's rare earth industry. Information Office of the State Council, The People's Republic of China
123. Wang L, Huang X, Yu Y, Zhao L, Wang C, Feng Z, Cui D, Long Z (2017) Towards cleaner production of rare earth elements from bastnaesite in China. J Clean Prod 165:231–242. https://doi.org/10.1016/j.jclepro.2017.07.107
124. Bergeron M, Langlais A, Ourriban M, Pelletier P (2016) Dry chlorination process to produce anhydrous rare earth chlorides. Patent EP-3077338-B1
125. Meshram RN (2011) Strategic value of Indian rare earth minerals. POSRI Chindia Q 2:103–110